Electronic Supplementary Material (ESI) for Physical Chemistry Chemical Physics.

Quantifying quadrupole effects in NMR spectra of spin-1/2 nuclei in rotating solids

Nisha Bamola, Mohit Bansal and Ramesh Ramachandran*

Department of Chemical Sciences
Indian Institute of Science Education and Research
(IISER) Mohali, Sector 81,Manauli P.O. Box-140306, Mohali, Punjab, India

1. Basic Theory

The Hamiltonian of an isolated three level system in the rotating frame is represented by the following equation.

$$\widetilde{H}(t) = \Delta\omega I_Z - \omega_1 I_X + \sum_{q=2}^{2} R_L^{(2)-q}(t) T^{(2)q} e^{iq\omega t} \tag{1}$$

In the above equation, $\Delta\omega = \omega - \omega_0$ represents the chemical shift offset in the rotating frame, while, 'ω_1' and 'ω' represent the amplitude and frequency of the oscillating magnetic field. The term 'ω_0' depicts the effective precessional frequency of the nucleus (in the presence of chemical shift interactions). The last term represents the quadrupolar interaction. For convenience, the quadrupolar interaction is commonly expressed in terms of irreducible spatial ($R^{(2)-q}$) and spin tensor operators ($T^{(2)q}$). Often the spatial tensors are defined in the principle axis systems (PAS)and are transformedinto the laboratory frame through a series of transformations employing the Wigner rotations matrices. Depending on the nature of these transformations, the form of the spatial coefficients differ and are summarised below.

$$R_L^{(2)q} = \sum_{m=\pm 2,0} R_{PAS}^{(2)m} D_{m,q}\left(\Omega_{PL}\right) \qquad \text{(for static single crystal)} \tag{2}$$

$$R_L^{(2)q} = \sum_{m,m=-2}^{2} R_{PAS}^{(2)m} D_{m,m}\left(\Omega_{PM}\right) D_{m,q}\left(\Omega_{ML}\right) \qquad \text{(for static powder sample)} \tag{3}$$

For the sake of continuity, a brief description of the spatial and spin tensor operators is given below.

$R_{Q,PAS}^{(2)0} = \omega_Q$, $R_{Q,PAS}^{(2)\pm 1} = 0$, $R_{Q,PAS}^{(2)\pm 2} = -\frac{\omega_Q \eta}{\sqrt{6}}$ ($\omega_Q = \frac{3(2\pi)}{2I(2I-1)} C_Q$,$C_Q = \frac{e^2 qQ}{h}$)

$T^{(2)0} = \frac{1}{\sqrt{6}}\left(3I_Z^2 - I^2\right)$, $T^{(2)\pm 1} = \mp\frac{1}{2}\left(I_Z I_\pm + I_\pm I_Z\right)$, $T^{(2)\pm 2} = \frac{1}{2} I_\pm^2$

Unlike the excitation in spin I=1/2 systems, the magnitude of the quadrupolar interactions (both time-dependent and time independent) in the rotating frame often exceeds the amplitude of the pulse often resulting in the selective excitation. Depending on the relative magnitudes of the quadrupolar frequency 'ω_Q' and the effective Larmor frequency 'ω_0' of the nucleus under study, the time-dependent terms (commonly referred to as"second-order" quadrupolar interactions) do play an important role in the excitation process and would be described in the following sections. To pedagogically outline the role of the various interactions terms (such as offsets, second-order quadrupolar interactions etc.) in the examination process (i.e. the excitation of double-quantum (DQ)transitions (transitions from m=1 to m=-1), we begin the discussion in the presence of both off-sets and second-order quadrupolar interactions under static conditions.

To facilitate analytic descriptions in multi-level systems and draw parallels with standard two-level systems (I=1/2), the Hamiltonian in the rotating frame is re-expressed in terms of the fictitious spin-operators.

$$\widetilde{H} = 2\left\{\omega - \left(\omega_0 - \frac{\omega_Q^{(1)}(\alpha\beta\gamma)}{6}\right)\right\} I_Z^{12} - \sqrt{2}\omega_1 I_X^{12} + 2\left\{\omega - \left(\omega_0 + \frac{\omega_Q^{(1)}(\alpha\beta\gamma)}{6}\right)\right\} I_Z^{23} - \sqrt{2}\omega_1 I_X^{23} \tag{4}$$

When the frequency of the oscillating field is adjusted to the precessional frequency of the nucleus under study (i.e. $\omega = \omega_0$), the above Hamiltonian reduces to the

$$\tilde{H} = \underbrace{\frac{\omega_Q^{(1)}(\alpha\beta\gamma)}{3} I_Z^{12} - \sqrt{2}\omega_1 I_X^{12}} - \underbrace{\frac{\omega_Q^{(1)}(\alpha\beta\gamma)}{3} I_Z^{23} - \sqrt{2}\omega_1 I_X^{23}} \tag{5}$$

In the above equation, $\omega_Q^{(1)}(\alpha\beta\gamma)$ denotes contributions from the first order quadrupolar interactions and is dependent on the nature of the sample under consideration (i.e. $\omega_Q^{(1)}(\alpha\beta\gamma) = R_L^{(2)0}$)

Since second-order quadrupolar interactions become relevant in systems with large quadrupolar coupling constants and plays an important role in the excitation process, the time-dependent contributions (due to quadrupolar interactions) in the rotating frame are incorporated through averaging methods.
Accordingly, the Hamiltonian in the rotating frame incorporating offsets and second-order quadrupolar interactions is represented by the following equations.

$$\tilde{H} = \underbrace{\frac{\omega_Q^{(1)}(\alpha\beta\gamma)}{3} I_Z^{12} - \sqrt{2}\omega_1 I_X^{12}} - \underbrace{\frac{\omega_Q^{(1)}(\alpha\beta\gamma)}{3} I_Z^{23} - \sqrt{2}\omega_1 I_X^{23}} + \left(\Delta\omega + \omega_Q^{(2)}(\alpha\beta\gamma)\right) 2I_Z^{13} \tag{6}$$

In the above equation, the term $\omega_Q^{(2)}(\alpha\beta\gamma)$ denotes the second-order quadrupolar correction and is represented by the following equation.

$$\omega_Q^{(2)}(\alpha\beta\gamma) = \frac{1}{12\omega_0}\left[R_L^{(2)1} R_L^{(2)-1} - R_L^{(2)2} R_L^{(2)-2}\right] \tag{7}$$

2. Additional Simulations

2.1 Effective fields in three level system

A. DQ excitation under on-resonance conditions (in the presence of first-order quadrupolar interactions)

In the simulations depicted below, the validity of the effective field approach is examined in systems with lower quadrupolar coupling constants (ranging from 25kHz to 500kHz) at different Rf amplitudes in both sungle crystal and powder samples.

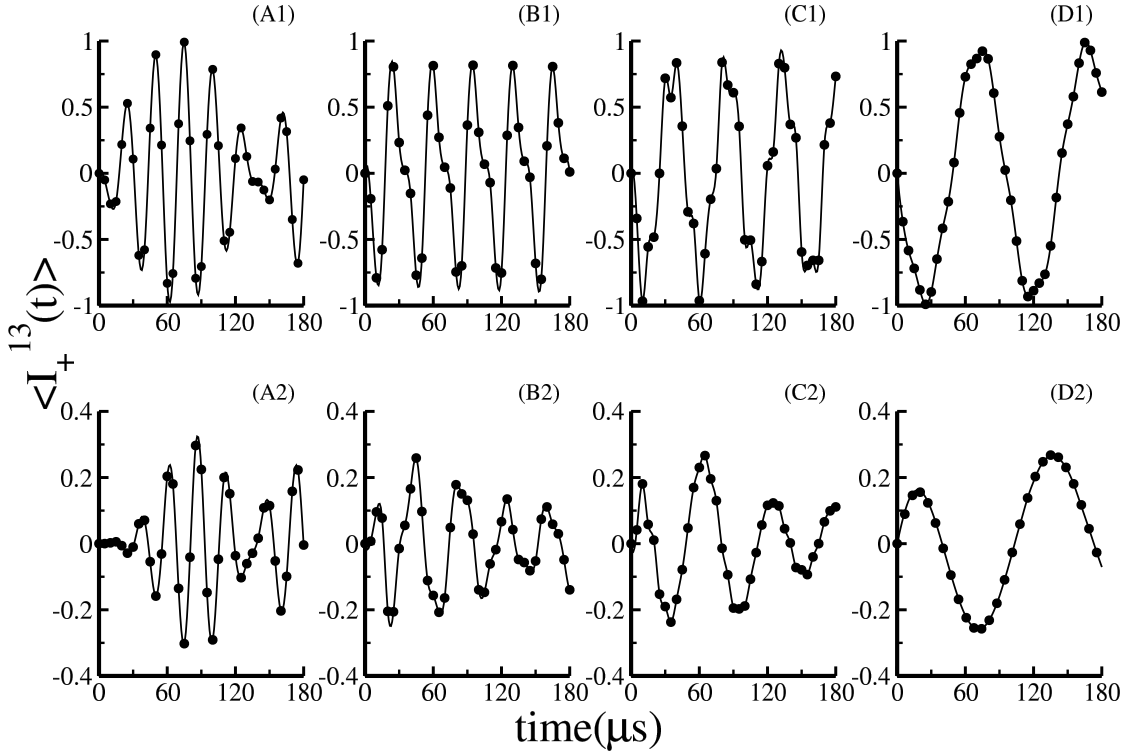

Figure S1: In the simulations depicted (first row (single crystal), second row (powder sample)), excitation profile for different C_Q (all regimes) in the presence of first order quadrupolar interaction is illustrated for a given RF amplitude, $\nu_1 = 40$ kHz. The following parameters are employed in the simulations: (A) $C_Q = 25$ kHz; (B) $C_Q = 100$ kHz; (C) $C_Q = 200$ kHz; (D) $C_Q = 500$ kHz. In all the simulations, the following quadrupolar parameters are employed:$\eta = 0, \Omega_{PM} = (30^\circ, 40^\circ, 60^\circ)$. The powder simulations were performed over 28656 orientations (zcw28656).

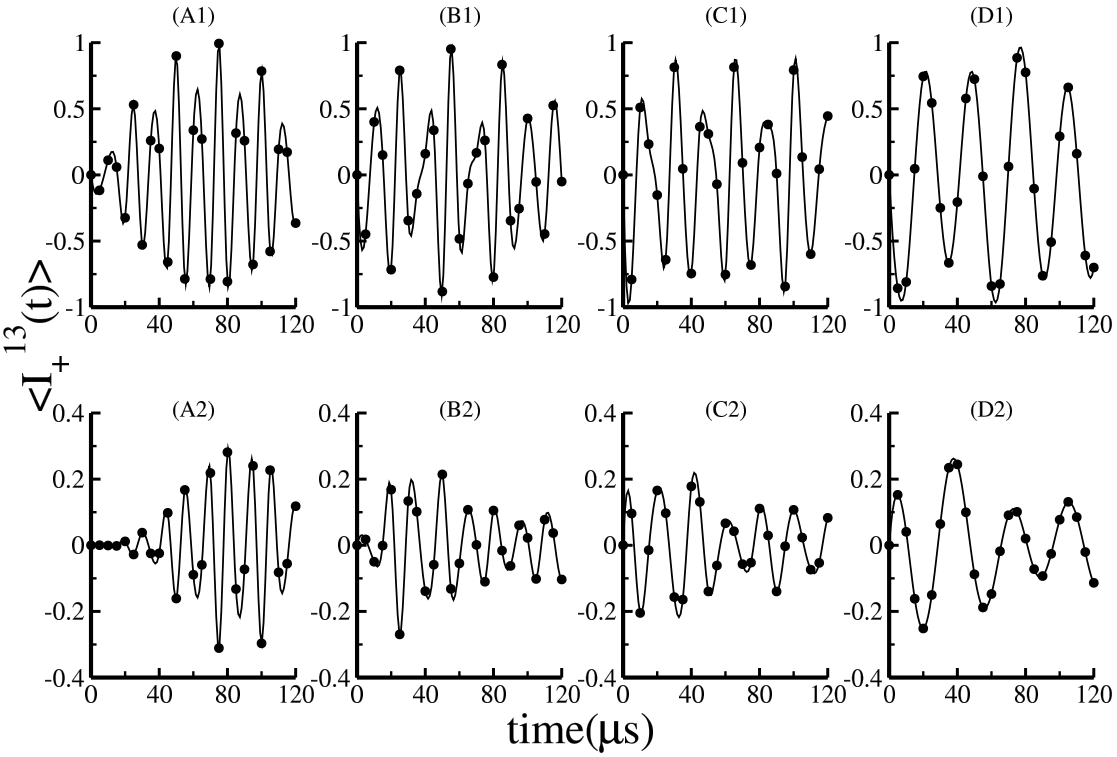

Figure S2: In the simulations depicted (first row (single crystal), second row (powder sample)), excitation profile for different C_Q (all regimes) in the presence of first order quadrupolar interaction is illustrated for a given RF amplitude, $\nu_1 = 80$ kHz. The following parameters are employed in the simulations: (A) $C_Q = 25$ kHz;(B) $C_Q = 100$ kHz;(C) $C_Q = 200$ kHz;(D) $C_Q = 500$ kHz. In all the simulations, the following quadrupolar parameters are employed: $\eta = 0, \Omega_{PM} = (30^\circ, 40^\circ, 60^\circ)$. The powder simulations were performed over 28656 orientations (zcw28656).

B. DQ excitation under off-resonance conditions (in the presence of both first and second-order quadrupolar interactions)

In the simulations depicted below, the role of the offsets in the compensation of second-order quadrupolar interactions is discussed in both single crystal and powder samples. To deduce the optimal value of the offset value in a powder sample, the orientation dependence of the second-order quadrupolar interactions in various crystallites is depicted below in Figure 3

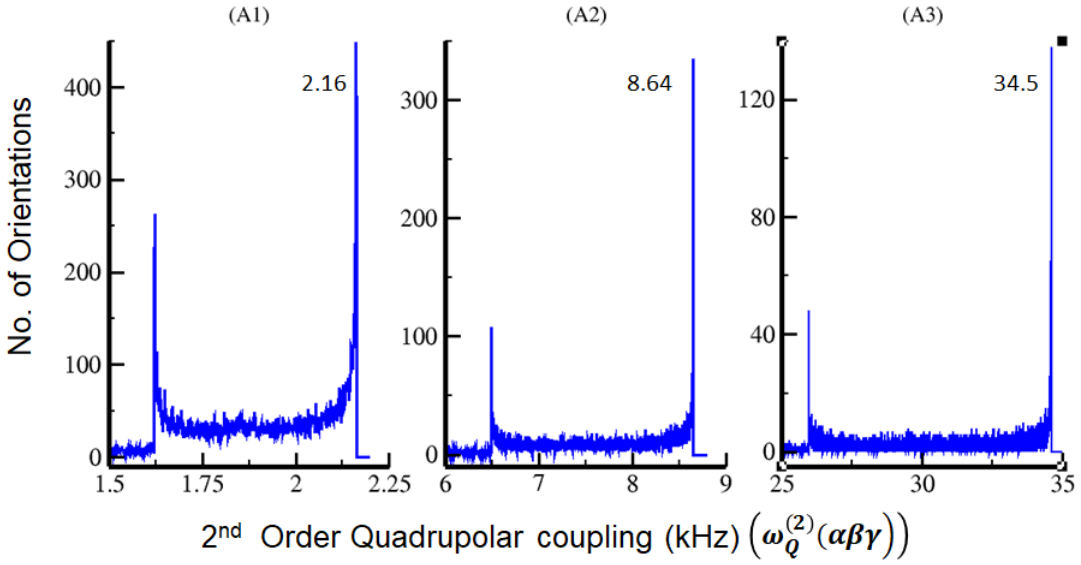

Figure S3: Figure depicts the distribution of second order quadrupolar couplings in a powder sample for different values of coupling constants. Quadrupolar coupling constant for different simulations are (A1) 1000 kHz; (A2) 2000 kHz; (A3) 4000 kHz. The powder simulations were performed over 28656 orientations

Based on the above simulations (Figure S3), the optimal value of the offsets in powder samples is deduced based on the contributions emerging from maximum number of crystallites in a powder samples. In the simulations depicted below, the off set compensation is examined at different RF amplitudes.

(i) Off set Compensation for C_Q=1 MHz (ν_1=40 kHz)

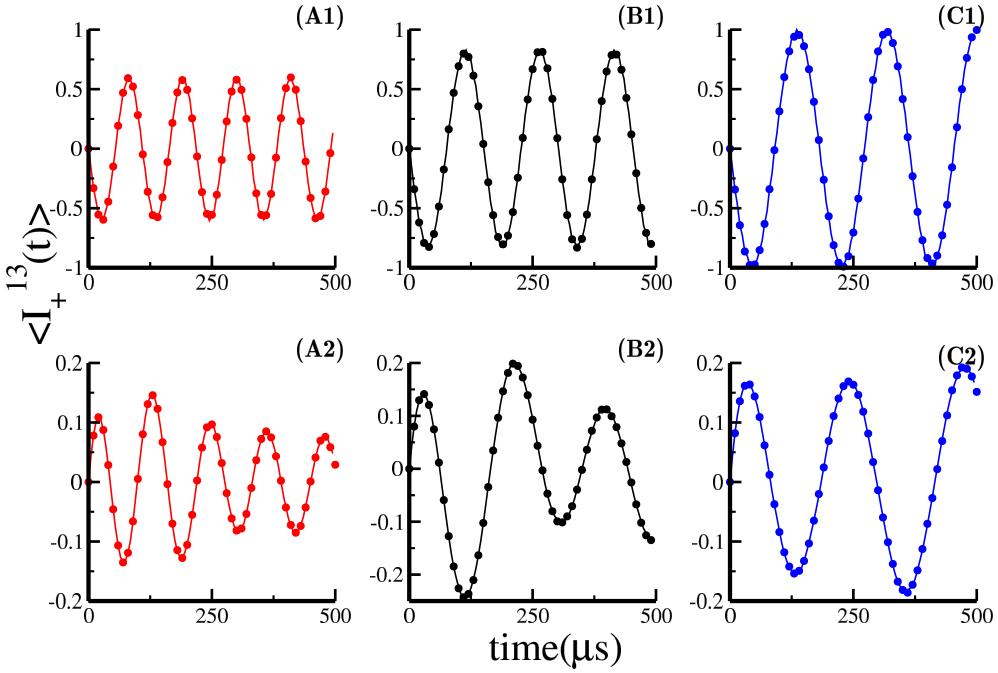

Figure S4: In the simulations depicted (first row (single crystal), second row (powder sample)), the role of offsets ($\Delta\omega = +ve(red)$, $\Delta\omega = 0(black)$ and $\Delta\omega = -ve(blue)$in the compensation of second order quadrupolar interactions is illustrated for a given RF amplitude, $\nu_1 = 40$ kHz. The following parameters are employed in the simulations: (A1) $\Delta\omega = 1.8$ kHz; (B1) $\Delta\omega = 0$ kHz; (C1) $\Delta\omega = -1.8$ kHz; (A2) $\Delta\omega = 2.16$ kHz; (B2) $\Delta\omega = 0$ kHz; (C2) $\Delta\omega = -2.16$ kHz. In all the simulations, the following quadrupolar parameters are employed: Cq=1.0 MHz, η= $0, \Omega_{PM} = (30°, 40°, 60°)$. The powder simulations were performed over 28656 orientations (zcw28656).

(i) Off set Compensation for C_Q=1 MHz (ν_1=80 kHz)

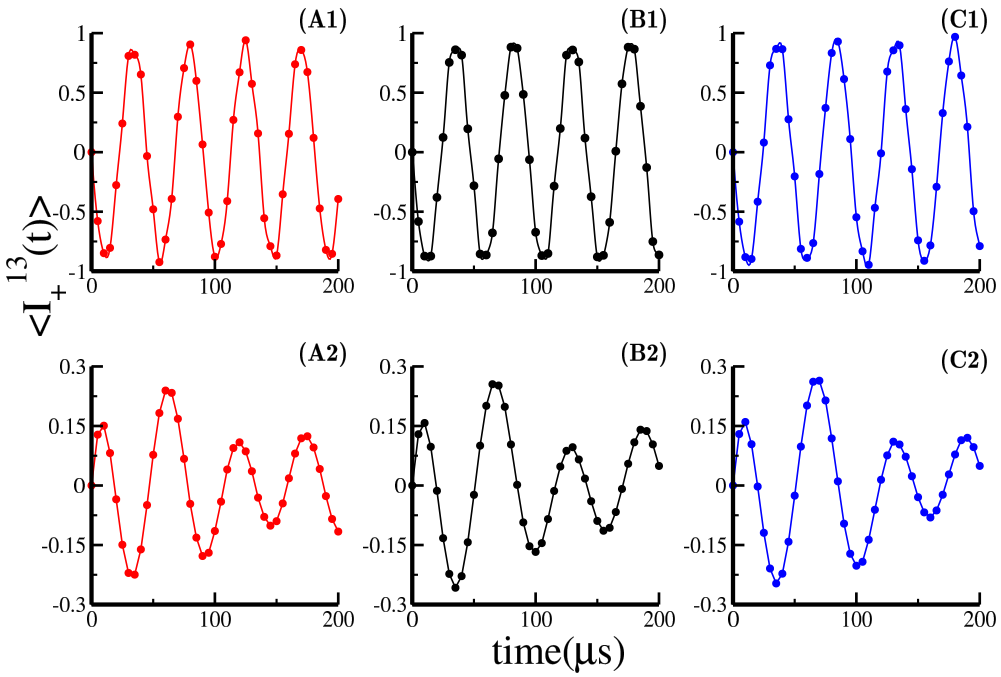

Figure S5: In the simulations depicted (first row (single crystal), second row (powder sample)), the role of offsets ($\Delta\omega = +ve(red)$,$\Delta\omega = 0(black)$ and $\Delta\omega = -ve(blue)$in the compensation of second order quadrupolar interactions is illustrated for a given RF amplitude, $\nu_1 = 80$ kHz. The following parameters are employed in the simulations: (A1) $\Delta\omega = 1.8$ kHz; (B1) $\Delta\omega = 0$ kHz; (C1) $\Delta\omega = -1.8$ kHz; (A2) $\Delta\omega = 2.16$ kHz; (B2) $\Delta\omega = 0$ kHz; (C2) $\Delta\omega = -2.16$ kHz. In all the simulations, the following quadrupolar parameters are employed: Cq=1.0 MHz, η= $0, \Omega_{PM} = (30^\circ, 40^\circ, 60^\circ)$. The powder simulations were performed over 28656 orientations (zcw28656).

(i) Off set Compensation for C_Q=2 MHz (ν_1=40 kHz)

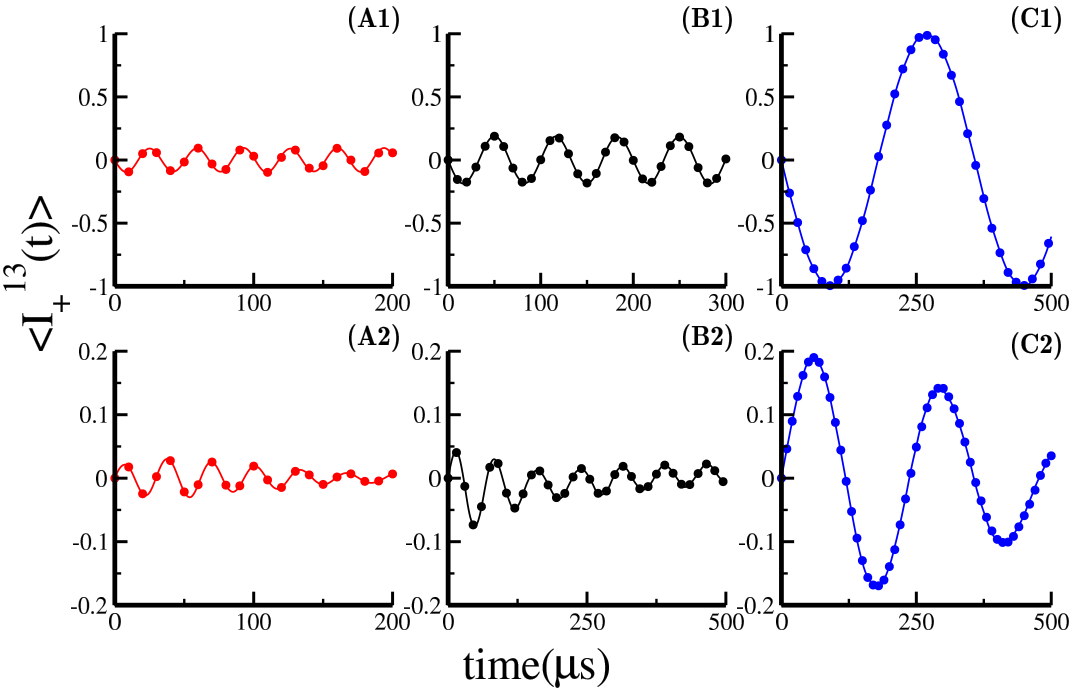

Figure S6: In the simulations depicted (first row (single crystal), second row (powder sample)), the role of offsets ($\Delta\omega = +ve(red)$, $\Delta\omega = 0(black)$ and $\Delta\omega = -ve(blue)$in the compensation of second order quadrupolar interactions is illustrated for a given RF amplitude, $\nu_1 = 40$ kHz. The following parameters are employed in the simulations: (A1) $\Delta\omega = 7.3$ kHz; (B1) $\Delta\omega = 0$ kHz; (C1) $\Delta\omega = -7.3$ kHz; (A2) $\Delta\omega = 8.64$ kHz; (B2) $\Delta\omega = 0$ kHz; (C2) $\Delta\omega = -8.64$ kHz. In all the simulations, the following quadrupolar parameters are employed: Cq=1.0 MHz, η= $0, \Omega_{PM} = (30^\circ, 40^\circ, 60^\circ)$. The powder simulations were performed over 28656 orientations (zcw28656).

(i) Off set Compensation for C_Q=2 MHz (ν_1=80 kHz)

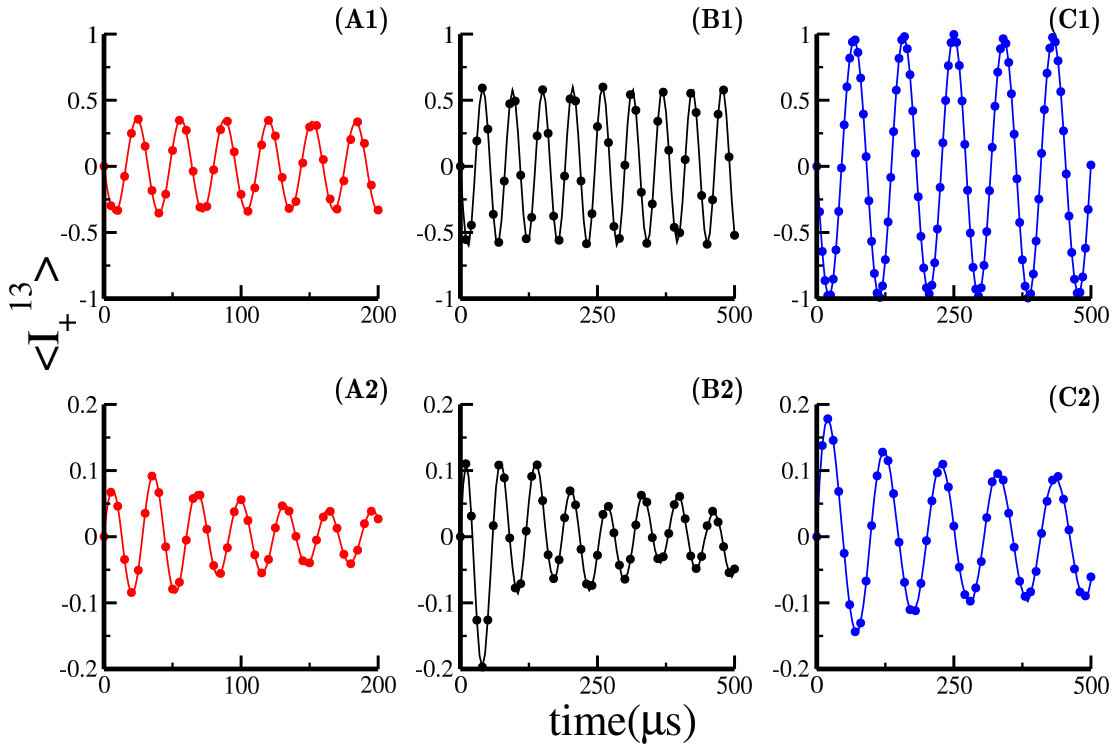

Figure S7: In the simulations depicted (first row (single crystal), second row (powder sample)), the role of offsets ($\Delta\omega = +ve(red)$, $\Delta\omega = 0(black)$ and $\Delta\omega = -ve(blue)$in the compensation of second order quadrupolar interactions is illustrated for a given RF amplitude, $\nu_1 = 80$ kHz. The following parameters are employed in the simulations: (A1) $\Delta\omega = 7.3$ kHz; (B1) $\Delta\omega = 0$ kHz; (C1) $\Delta\omega = -7.3$ kHz; (A2) $\Delta\omega = 8.64$ kHz; (B2) $\Delta\omega = 0$ kHz; (C2) $\Delta\omega = -8.64$ kHz. In all the simulations, the following quadrupolar parameters are employed: Cq=1.0 MHz, η= $0, \Omega_{PM} = (30^\circ, 40^\circ, 60^\circ)$. The powder simulations were performed over 28656 orientations (zcw28656).

(i) Off set Compensation for C_Q=4 MHz (ν_1=40 kHz)

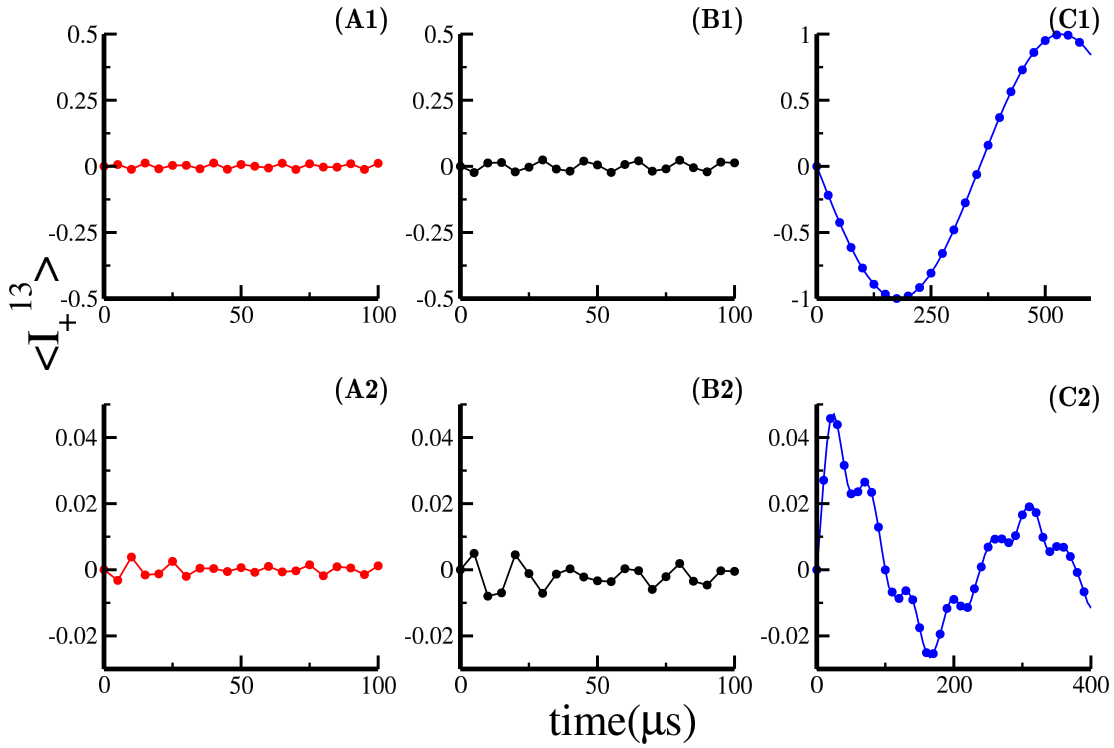

Figure S8: In the simulations depicted (first row (single crystal), second row (powder sample)), the role of offsets ($\Delta\omega = +ve(red)$, $\Delta\omega = 0(black)$ and $\Delta\omega = -ve(blue)$in the compensation of second order quadrupolar interactions is illustrated for a given RF amplitude,$\nu_1 = 40$ kHz. The following parameters are employed in the simulations: (A1) $\Delta\omega = 24.5$ kHz; (B1) $\Delta\omega = 0$ kHz; (C1) $\Delta\omega = -24.5$ kHz; (A2) $\Delta\omega = 34.59$ kHz;(B2) $\Delta\omega = 0$ kHz; (C2) $\Delta\omega = -34.59$ kHz. In all the simulations, the following quadrupolar parameters are employed: Cq=4.0 MHz,η= 0,$\Omega_{PM} = (30^\circ, 40^\circ, 60^\circ)$. The powder simulations were performed over 28656 orientations (zcw28656).

(i) Off set Compensation for C_Q=4 MHz (ν_1=80 kHz)

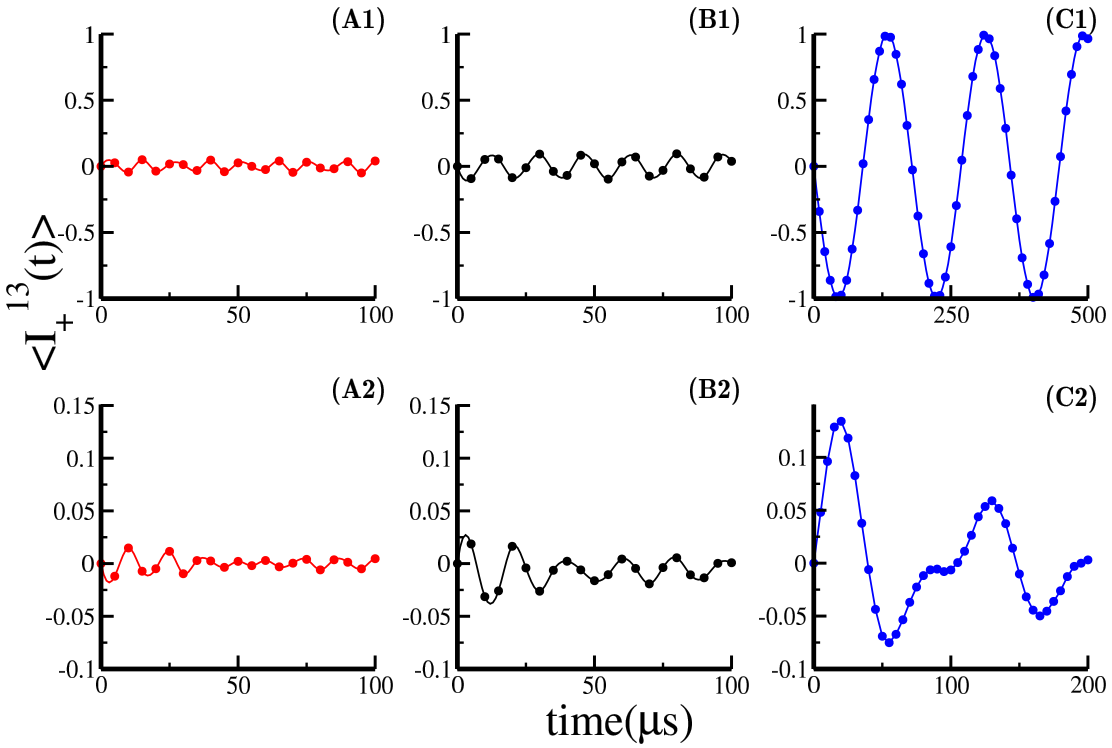

Figure S9: In the simulations depicted (first row (single crystal), second row (powder sample)), the role of offsets ($\Delta\omega = +ve(red)$, $\Delta\omega = 0(black)$ and $\Delta\omega = -ve(blue)$in the compensation of second order quadrupolar interactions is illustrated for a given RF amplitude, $\nu_1 = 80$ kHz. The following parameters are employed in the simulations: (A1) $\Delta\omega = 24.5$ kHz; (B1) $\Delta\omega = 0$ kHz; (C1) $\Delta\omega = -24.5$ kHz; (A2) $\Delta\omega = 34.59$ kHz;(B2) $\Delta\omega = 0$ kHz; (C2) $\Delta\omega = -34.59$ kHz. In all the simulations, the following quadrupolar parameters are employed: Cq=4.0 MHz, η= 0,, $\Omega_{PM} = (30^\circ, 40^\circ, 60^\circ)$. The powder simulations were performed over 28656 orientations (zcw28656).

2.2 Effective fields in coupled system (I=1/2,S=1)

In the simulations depicted below, a comparison of the time-domain and frequency-domain signal emerging from analytic and numerical methods is illustrated.

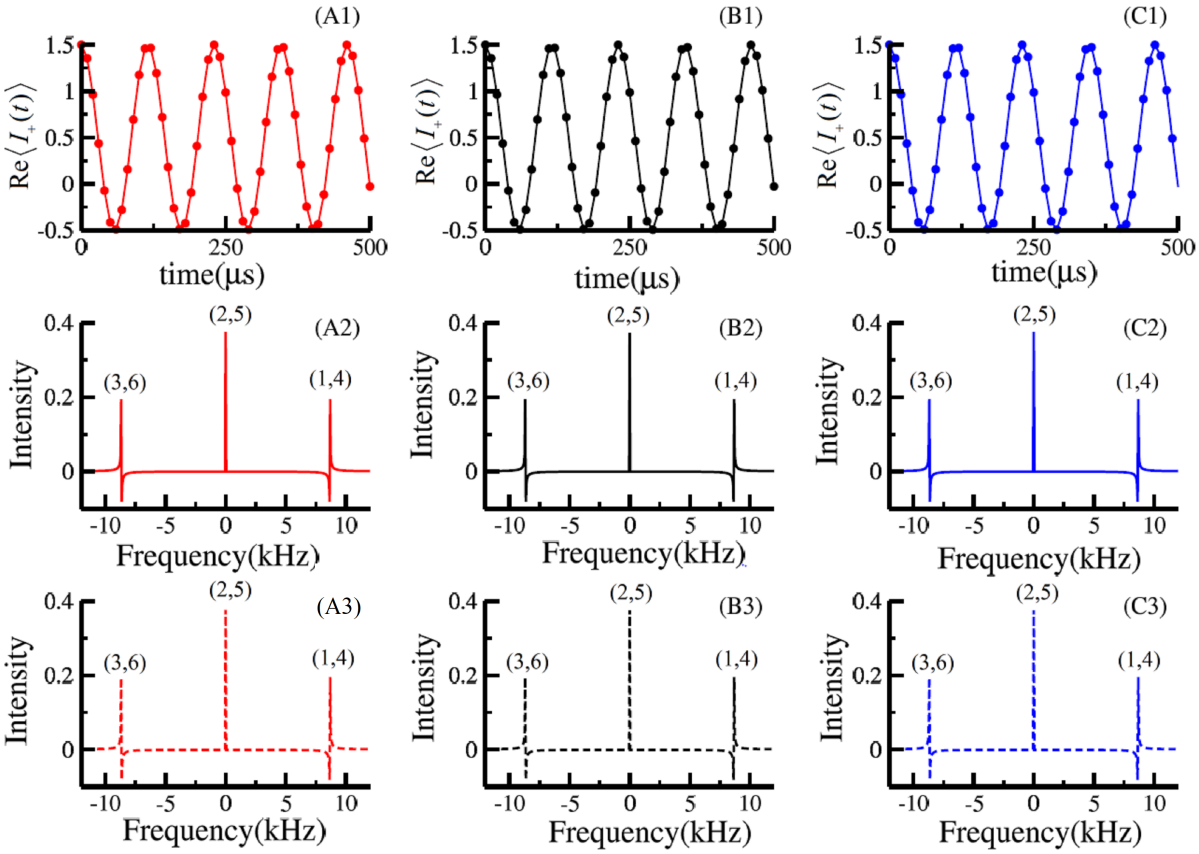

Figure S10: In the simulations depicted, the role of off-sets is varied along the column ($\Delta\omega_S = 0.72$ kHz (first column), $\Delta\omega_S = 0$ kHz (second column), $\Delta\omega_S = -0.72$ kHz (third column)). Numerical simulations are depicted through solid lines and analytical results are depicted through dots (first row) and dashed lines (third row). All the simulations contain second order quadrupolar interactions. In all the simulations, the following parameters were employed: dipolar coupling constant, ω_{IS}=8.6 kHz, C_Q=1 MHz, η= 1.0, $\Omega_{PM} = (0°, 90°, 0°)$, $\nu_{RF,S} = 0$ kHz.

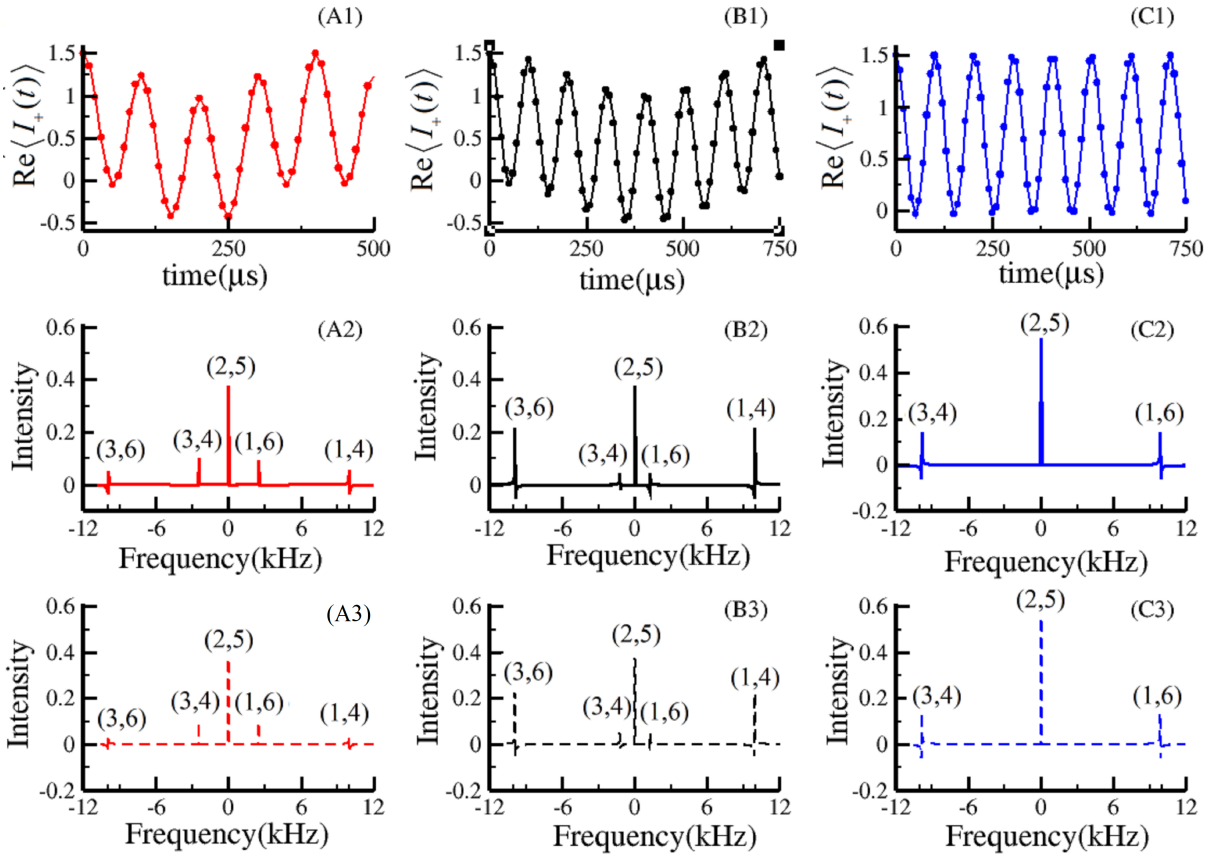

Figure S11: In the simulations depicted, the role of off-sets is varied along the column ($\Delta\omega_S = 0.72$ kHz (first column), $\Delta\omega_S = 0$ kHz (second column), $\Delta\omega_S = -0.72$ kHz (third column)). Numerical simulations are depicted through solid lines and analytical results are depicted through dots (first row) and dashed lines (third row). All the simulations contain second order quadrupolar interactions. In all the simulations, the following parameters were employed: ω_{IS}=8.6 kHz, C_Q=1 MHz, η= 1.0, $\Omega_{PM} = (0°, 90°, 0°)$, $\nu_{RF,S} = 60$ kHz

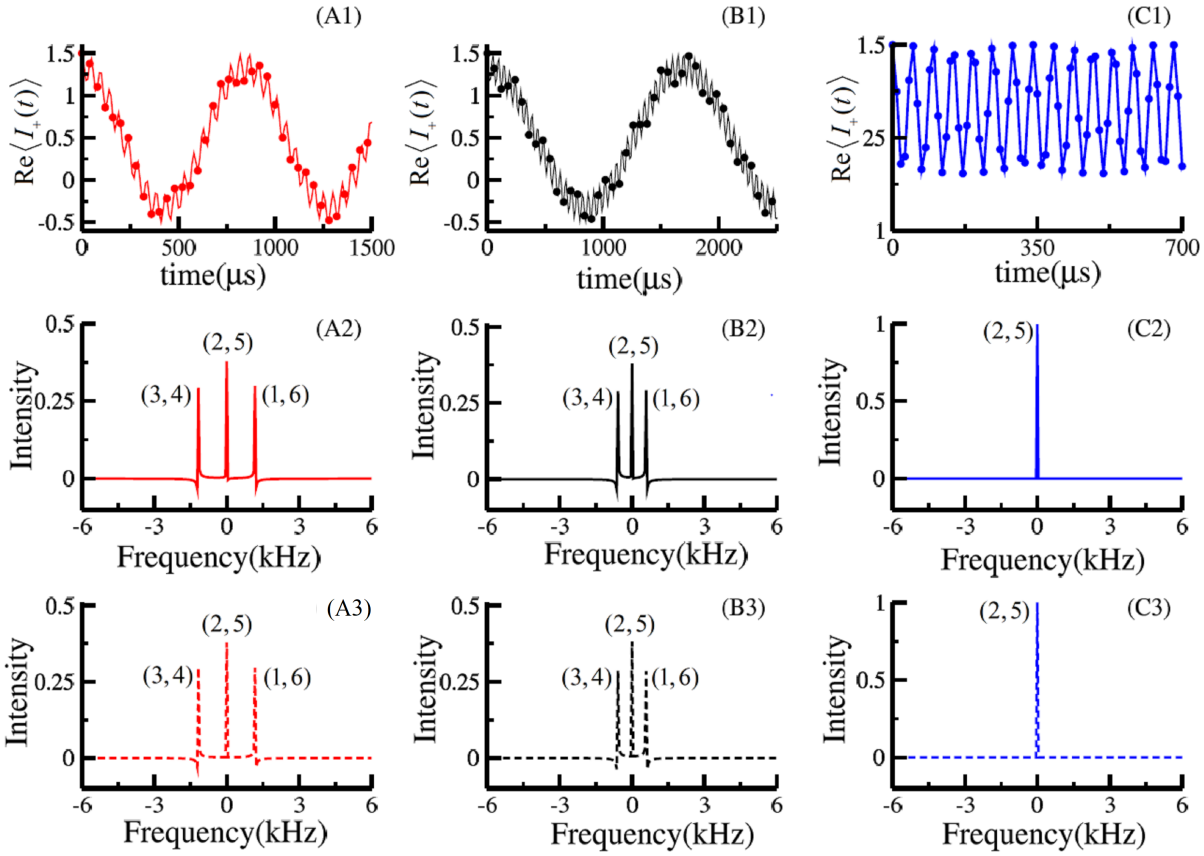

Figure S12: In the simulations depicted, the role of off-sets is varied along the column ($\Delta\omega_S = 0.72$ kHz (first column), $\Delta\omega_S = 0$ kHz (second column), $\Delta\omega_S = -0.72$ kHz (third column)). Numerical simulations are depicted through solid lines and analytical results are depicted through dots (first row) and dashed lines (third row). All the simulations contain second order quadrupolar interactions. In all the simulations, the following parameters were employed: ω_{IS}=8.6 kHz, C_Q=1 MHz, η= 1.0, $\Omega_{PM} = (0°, 90°, 0°)$, $\nu_{RF,S} = 120$ kHz

2.3 Effective fields in rotating solids

In MAS experiments, the anisotropic components of the internal interactions (CSA, dipolar and quadrupolar interaction) are represented through the following standard expression.

$$\omega_\lambda^{(m)} = \sum_{m_1=-2}^{2} R_{P,\lambda}^{(2)m_1} \sum_{m_2=-2}^{2} D_{m_1 m_2}\left(\Omega_{PM}\right) D_{m_2 m}\left(\Omega_{MR}\right) d_{m0}\left(\beta_{RL}\right) \tag{8}$$

Here, $R_{P,\lambda}^{(2)m_1}$ represents the component of the spatial tensor (λ= CSA, dipolar or quadrupolar interaction) defined in the principal axis system (PAS), while $D_{m_1 m_2}\left(\Omega_{AB}\right)$ denotes the Wigner Rotation matrix. In the principal axis system, the R-coefficients of various interactions are defined as follows.

$$R_{P,CSA}^{(2)0} = \delta_{aniso}\ ,\ R_{P,CSA}^{(2)\pm2} = -\frac{1}{\sqrt{6}}\delta_{aniso}\eta\ ,\ R_{P,CSA}^{(2)\pm1} = 0 \tag{9}$$

$$R_{P,dipolar}^{(2)0} = \sqrt{6}b\left(b = -\frac{\mu_0\gamma_I\gamma_S}{4\pi r_{IS}^3}\right)\ ,\ R_{P,dipolar}^{(2)\pm2} = R_{P,dipolar}^{(2)\pm1} = 0 \tag{10}$$

$$R_{P,Quad}^{(2)0} = \omega_Q\ ,\ R_{P,Quad}^{(2)\pm2} = -\frac{1}{\sqrt{6}}\omega_Q\eta\left(\omega_Q = 2\pi\frac{3C_Q}{2I(2I-1)}, C_Q = e^2qQ\right)\ ,\ R_{P,Quad}^{(2)\pm1} = 0 \tag{11}$$

The coefficients ($A_{X,p}$ and $B_{Y,p}$) in the time-dependent rf part can be expressed in terms of bessel functions as.

$$A_{X,p} \propto \sum_{n_1} J_{n_1}\left(A_1\right) \sum_{n_2} J_{n_2}\left(A_2\right) \sum_{n_3} J_{n_3}\left(A_3\right) \sum_{n_4} J_{n_4}\left(A_4\right)\ ;\ n_1 + n_2 + n_3 + n_4 = p \tag{12}$$

$$B_{Y,p} \propto \sum_{n_1} J_{n_1}(A_1) \sum_{n_2} J_{n_2}(A_2) \sum_{n_3} J_{n_3}(A_3) \sum_{n_4} J_{n_4}(A_4)\ ;\ n_1+n_2+n_3+n_4 = p \tag{13}$$

$$A_1 = \frac{\omega_Q^{(1)} - \omega_Q^{(-1)}}{2i\omega_r}\ ,\ A_2 = \frac{\omega_Q^{(1)} + \omega_Q^{(-1)}}{2\omega_r}\ ,\ A_3 = \frac{\omega_Q^{(2)} - \omega_Q^{(-2)}}{4i\omega_r}\ ,\ A_4 = \frac{\omega_Q^{(2)} + \omega_Q^{(-2)}}{4\omega_r}$$